

Article

Numerical Study of the Effects of Heat Loss and Solid Thermal Conductivity on Syngas Production for Fuel Cells

Xiaolong Wang ¹, Mengmeng Yu ¹, Zunmin Li ¹, Zhen Wang ¹, Xiuxia Zhang ^{1,*}, Junrui Shi ², Xiangjin Kong ² and Jinsheng Lv ²

¹ Ocean College, Binzhou Polytechnic, Binzhou 256603, China; dmuxlwang@126.com (X.W.); yumengmeng1@bzpt.edu.cn (M.Y.); lizunmin1@bzpt.edu.cn (Z.L.); wangzhen@bzpt.edu.cn (Z.W.)

² School of Transportation and Vehicle Engineering, Shandong University of Technology, Zibo 255049, China; junruishibz@126.com (J.S.); kongxj@sut.edu.cn (X.K.); lvjinsheng@sut.edu.cn (J.L.)

* Correspondence: xiuxiazhang123@126.com

Abstract: Syngas can be used as feedstock for efficient energy conversion in solid oxide fuel cells (SOFCs). In the current paper, the conversion efficiency of methane to synthesis gas (H_2 and CO) within a two-layer porous media reactor is investigated by a one-dimensional two-temperature model. A detailed chemical reaction mechanism GRI-Mech 1.2 is used to describe the chemical processes. Attention is focused on CO_2 content in the methane/air mixture, heat loss to the surroundings, and solid thermal conductivity on temperature distribution and conversion efficiency. Numerical results show that addition of CO_2 to the methane/air mixture improves the conversion efficiency. For a molar ratio of $CO_2/CH_4 = 1$, the conversion efficiency reaches 44.8%. An increase in heat loss to the surroundings leads to a decrease in conversion efficiency. A greater solid thermal conductivity can improve the conversion efficiency.

Keywords: two-layer porous media reactor; CO_2 injection; heat loss; conversion efficiency



Academic Editor: Manickam

Minakshi

Received: 12 March 2025

Revised: 6 May 2025

Accepted: 8 May 2025

Published: 9 May 2025

Citation: Wang, X.; Yu, M.; Li, Z.; Wang, Z.; Zhang, X.; Shi, J.; Kong, X.; Lv, J. Numerical Study of the Effects of Heat Loss and Solid Thermal Conductivity on Syngas Production for Fuel Cells. *Batteries* **2025**, *11*, 187. <https://doi.org/10.3390/batteries11050187>

Copyright: © 2025 by the authors. Licensee MDPI, Basel, Switzerland. This article is an open access article distributed under the terms and conditions of the Creative Commons Attribution (CC BY) license (<https://creativecommons.org/licenses/by/4.0/>).

1. Introduction

Solid oxide fuel cells (SOFCs) offer advantages such as high efficiency and environmental friendliness. Compared to traditional power generation methods, SOFCs can achieve a power generation efficiency of up to 60% and do not emit pollutants like NO_x , making them highly environmentally friendly.

The syngas for SOFCs is mostly obtained through the cracking of hydrocarbon fuel/air mixtures. H_2 has the advantages of high calorific value per unit mass and almost no environmental pollution during combustion. Hence, it is considered as an alternative to hydrocarbon fuel in the future. Although the reserves of H_2 are very rich, most of them exist in water and hydrocarbon fuels in the form of ions, which need to be extracted by certain means [1–4]. The primary methods for producing syngas include thermochemical water decomposition, biomass processing, electrolysis, coal and biogas utilization, steam reforming, partial oxidation, and autothermal reforming. Among these, the most prevalent method is the production of syngas through the reforming of hydrocarbon fuels [5,6].

Enhancing the conversion efficiency of hydrocarbon fuels is a hot topic in the field of SOFCs. Among various methods, the most advanced approach is to modify anodes by an active and stable coking catalytic layer as considered in the review by L. Fan et al. [7]. Another well-known approach is to transform fuel into syngas in the reactor with structured catalysts on heat-conducting substrates with nanocomposite active components possessing a high oxygen mobility and stability to coking [8]. The partial oxidation of rich fuels in

porous media represents a promising technology. The porous media reactor has garnered significant attention due to its extensive internal surface area and intricate gas flow pathways, which enhance heat transfer between the gas and solid phases. Syngas production by partial oxidation of fuel rich in porous media has been extensively studied [9,10].

Toledo et al. [11] carried out an experimental study on syngas production in inert porous media for three different hydrocarbon fuels. A one-dimensional steady-state numerical model was established by using the two-temperature model and a GRI-Mech 3.0 detailed chemical reaction mechanism. The critical equivalence ratio of the three fuels for superadiabatic combustion was presented. Araya et al. [12] conducted experimental and theoretical studies on syngas production in an inert porous medium composed of Al_2O_3 spheres by adding a certain proportion of water vapor into natural gas. They found that the output of H_2 increases with the increase in the proportion of steam in the mixture. Zeng et al. [13,14] carried out an experimental study on the fuel-rich combustion characteristics of a two-layer reactor by adding different proportions of CO_2 into a CH_4/air mixture, and they established a one-dimensional, steady-state, two-temperature model. The Peter mechanism of 17 species and 58 elementary reactions was adopted in their computations. The radiation heat loss of solids at the inlet and outlet to the environment was considered. Their results showed that CO_2 injection can improve the conversion efficiency of syngas.

In the experiment, heat loss to the surroundings is inevitable and the solid thermal conductivity may have significant influence on combustion characteristics and syngas production. Therefore, in the process of numerical studies, the wall heat loss should be considered and the appropriate heat loss coefficient should be selected to reflect the actual combustion situation of the reactor. Although fuel-lean [15,16] and fuel-rich [17–20] combustion in porous media has been numerically investigated, these effects have not been fully considered in previous research. The performance and durability of a 100 W SOFC stack system was investigated by Alenazey et al. [21] under the conditions of steady-state and current load cycling. It was found that the total degradation rates were 54, 297, and 370 mV within 72 h for three different stack temperatures of 650, 700, and 750 °C, respectively. However, a steady drop as small as 0.5% was observed during the 24 current load cycles.

This paper aims to clarify the effects of heat loss and thermal conductivity on syngas production. The research results provide guidance for improving conversion efficiency through optimized combustion conditions. To this end, a one-dimensional two-temperature steady-state model of a two-layer porous medium reactor is established. The two-temperature model means that the gas and solid phases have their own temperatures. The GRI-Mech 1.2 detailed mechanism [22] is adopted to deal with the methane/air combustion in porous media. Different proportions of CO_2 are added to the methane/air mixture to explore the effect of CO_2 injection on conversion efficiency. A heat loss coefficient is introduced to account for the heat loss to the surroundings and its influence on syngas production. The impact of material properties on conversion efficiency is also examined.

2. Mathematical Model

2.1. Model Description

The research object of this paper is a two-layer porous medium reactor designed by Zeng et al. [14]. The inner diameter of the reactor is 30 mm, and its length is 80 mm, as illustrated in Figure 1. The porous medium material used in the reactor is Al_2O_3 balls. The balls used in the upstream section have a diameter of 2–3 mm, a filling height of 20 mm, and a porosity of 0.4, serving as the diffusion layer for the flame. In the downstream section, the balls have a diameter of 7.5 mm, a filling height of 60 mm, and a porosity of 0.46, functioning as the flame-supporting layer. For simplification, it is assumed that the

diameter of the balls in the upstream section is 2.5 mm. The fuel used in the model is a methane/air mixture with varying proportions of CO₂.

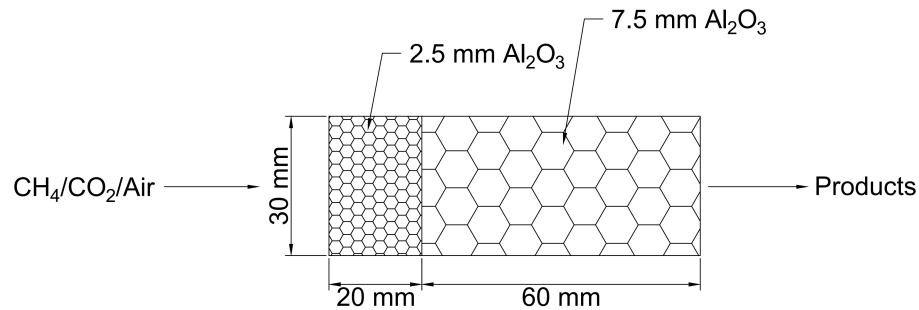


Figure 1. Schematic of the two-layer reactor.

2.2. Governing Equation

In this paper, a one-dimensional model of the reactor is established. Considering the complexity of heat transfer between the gas and solid phases in the reactor, the model is simplified with the following assumptions:

1. Gas radiation is ignored;
2. Porous media are isotropic and have an inert optical thickness;
3. The gas in porous media is an ideal gas and the flow in porous media is laminar;
4. A heat loss coefficient β is used to account for the heat loss to the surroundings.

Based on the above assumptions, the following governing equations are established [15].

Continuity equation:

$$\frac{d(\varepsilon \rho_g u_g)}{dx} = 0 \quad (1)$$

where ε is the porosity, and ρ_g and u_g are the gas density and mixture velocity, respectively.

Momentum equation:

$$\frac{d(\varepsilon \rho_g u_g u_g)}{dx} = -\varepsilon \frac{dp}{dx} + \frac{d}{dx} \left(\mu \frac{du_g}{dx} \right) - \frac{\Delta p}{\Delta x} \quad (2)$$

Gas energy equation:

$$\frac{d(\varepsilon \rho_g c_g u_g T_g)}{dx} - \sum_k \rho_g \varepsilon Y_k c_{gk} \left(D_{km} \frac{dY_k}{dx} \right) \frac{dT_g}{dx} = \frac{d}{dx} \left(\lambda_g \varepsilon \frac{dT_g}{dx} \right) - h_v (T_g - T_s) - \varepsilon \sum_k W_k h_k \omega_k \quad (3)$$

where c_g is the specific heat of the gas mixture, λ_g is the thermal conductivity of the gas mixture, ω_k and W_k are the reaction rate and molecular weight of the i -th component in the mixture, and h_v is the volumetric convective heat transfer coefficient, which is calculated by the following equations [15]:

$$h_v = \frac{6 N u_v S \lambda_g}{d^2} \quad (4)$$

$$N u_v = 2 + 1.1 P r^{1/3} R e^{0.6} \quad (5)$$

Solid energy equation:

$$\frac{d}{dx} \left((\lambda_s + \lambda_{rad}) \frac{dT_s}{dx} \right) + h_v (T_g - T_s) - \beta (T_s - T_0) = 0 \quad (6)$$

where β is the heat loss coefficient, and λ_{rad} is the radiative thermal conductivity of Al_2O_3 spheres.

$$\lambda_{\text{rad}} = \frac{32\varepsilon\sigma d}{9(1-\varepsilon)} T_s^3 \quad (7)$$

Species conservation equation:

$$\frac{d}{dx}(\varepsilon\rho_g Y_k u_g) = \frac{d}{dx}\left(\varepsilon\rho_g D_{km} \frac{dY_k}{dx}\right) + \varepsilon\dot{\omega}_k W_k \quad (8)$$

where Y_k is the mass fraction of the k -th component in the gas mixture.

The equation of state for an ideal gas is as follows:

$$P = \rho_g R T_g \quad (9)$$

where R is the general constant of gas. The gas density is obtained from the ideal gas equation. The gas property parameters are computed using the Chemkin and Transport packages provided by Kee et al. [23].

2.3. Boundary Conditions

The boundary conditions used in the model are given as follows.

Reactor inlet:

$$u_g = u_{g,\text{in}}, Y_k = Y_{k,\text{in}}, T_g = T_{g,\text{in}}, (\lambda_s + \lambda_{\text{rad}}) \frac{dT_s}{dx} = -\xi\sigma(T_s^4 - T_0^4) \quad (10)$$

Reactor outlet:

$$\frac{du_g}{dx} = \frac{dY_k}{dx} = \frac{dT_g}{dx} = \frac{dT_s}{dx} = 0, (\lambda_s + \lambda_{\text{rad}}) \frac{dT_s}{dx} = -\xi\sigma(T_s^4 - T_0^4) \quad (11)$$

Here, ξ is the surface emissivity of porous media.

2.4. Parameter Definition

The conversion efficiency of syngas is specified as

$$\eta = \frac{Y_{\text{H}_2,\text{out}} \times \text{LHV}_{\text{H}_2} + Y_{\text{CO},\text{out}} \times \text{LHV}_{\text{CO}}}{Y_{\text{CH}_4,\text{in}} \times \text{LHV}_{\text{CH}_4}} \quad (12)$$

where LHV is the low calorific value of components.

2.5. Chemical Mechanism

The chemical reaction mechanism has a significant effect on the temperature distribution and composition in porous media. The simplified mechanism is not sufficient to fully account for the partial combustion of methane in the reactor. Therefore, the detailed chemical reaction mechanism of GRI-Mech 1.2 is adopted in this paper, which consists of 32 species and 175 elementary reactions. ANSYS 15.0 is used in the numerical calculation.

2.6. Meshing and Solution Strategy

Based on the volume-averaged method, the burner is simplified as a regular geometric shape. A uniform square grid of 0.25 mm is applied throughout the computational domain, and a grid independence test is performed. The commercial software Fluent 15.0 is employed to solve the conservation equations with prescribed boundary conditions. The pressure–velocity coupling utilizes the SIMPLE algorithm. Second-order difference schemes are adopted for the gas and solid energy equations and the momentum equation. To simulate methane ignition, a 20 mm long high-temperature zone (1800 K) is initialized

at the interface between sections. The convergence criteria are set to 1×10^{-6} for energy equations and 1×10^{-3} for other equations.

3. Results and Analysis

3.1. Effect of CO₂ Injection

In this paper, the volume flow rate and equivalence ratio of air are fixed at 5 L/min and 1.5, respectively. Figure 2 depicts the gas and solid temperatures for four different molar ratios of CO₂/CH₄. It is evident that the gas temperature increases sharply within the reaction zone. The heat released during combustion is rapidly transferred to the solid porous media through convection heat transfer, resulting in a swift increase in solid temperature as well. However, a temperature difference exists between the gas and solid phases, which is referred to as the thermal nonequilibrium phenomenon. Consequently, it is necessary to model the energy equations for gas and solid separately in the numerical study. In the upstream of the combustion zone, the solid temperature is higher than the gas temperature, and the fresh mixture is preheated by the solid porous media. In the combustion area, the gas temperature rises above that of the solid temperature. In the downstream of the combustion area, the temperature difference between the gas and the solid gradually decreases, indicating that heat is being transferred from the gas to the solid [24].

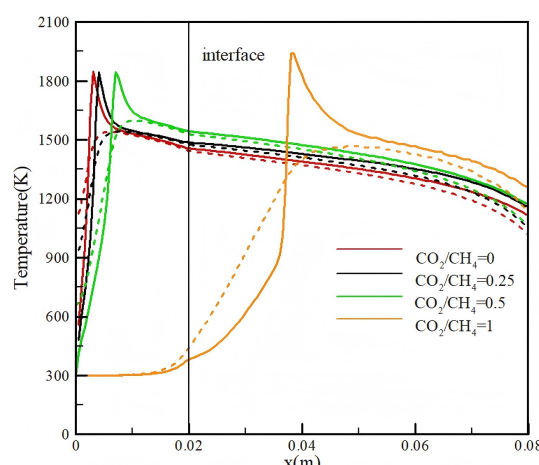


Figure 2. Temperature distributions for different molar ratios of CO₂/CH₄ (solid line presents gas temperature T_g; dashed line presents solid temperature T_s).

As the molar ratio of CO₂/CH₄ increases from 0 to 1, the flame front gradually moves downstream. Specifically, when the molar ratio of CO₂/CH₄ reaches 1, the flame is located approximately 17 mm downstream of the interface between the two sections, and the peak gas temperature reaches 1950 K. The preheating zone is lengthened, and more heat is stored in the solid matrix, which enhances the preheating effect on the fresh mixture, resulting in an increase in the peak gas temperature. As the molar ratio of CO₂/CH₄ increases, the temperature difference between the gas and solid phases also increases. This phenomenon can be attributed to two main reasons. Firstly, increasing the proportion of CO₂ injection leads to an increase in the inlet air velocity, which shortens the residence time of the gas in the porous media and weakens the heat transfer effect between the gas and solid. Secondly, as the flame propagates downstream, the diameter of the small ball increases to 7.5 mm. With the increase in the diameter of the ball, the convective heat transfer coefficient decreases under the same conditions.

Figure 3 illustrates the mole fraction of the main components near the reaction zone for molar ratios of CO₂/CH₄ = 0 and 1. The chemical reaction occurs in a very narrow

area, approximately 3 mm thick. Within the reaction zone, the mole fractions of CH_4 and O_2 decrease rapidly, indicating that the combustion reaction is taking place. The main components of syngas quickly reach their peak values and remain stable. For molar ratios of $\text{CO}_2/\text{CH}_4 = 0$ and 1, the distribution of each component is similar, except for CO_2 in the reaction zone. For a molar ratio of $\text{CO}_2/\text{CH}_4 = 1$, the mole fraction of CO_2 initially decreases through the main elementary reaction reactions $2\text{H} + \text{CO}_2 \leftrightarrow \text{H}_2 + \text{CO}_2$ and $\text{CH} + \text{CO}_2 \leftrightarrow \text{HCO} + \text{CO}$, and then increases via elementary reaction $\text{O}_2 + \text{CO} \leftrightarrow \text{O} + \text{CO}_2$, suggesting that CO_2 first participates in the reaction as a reactant and is subsequently generated as a product.

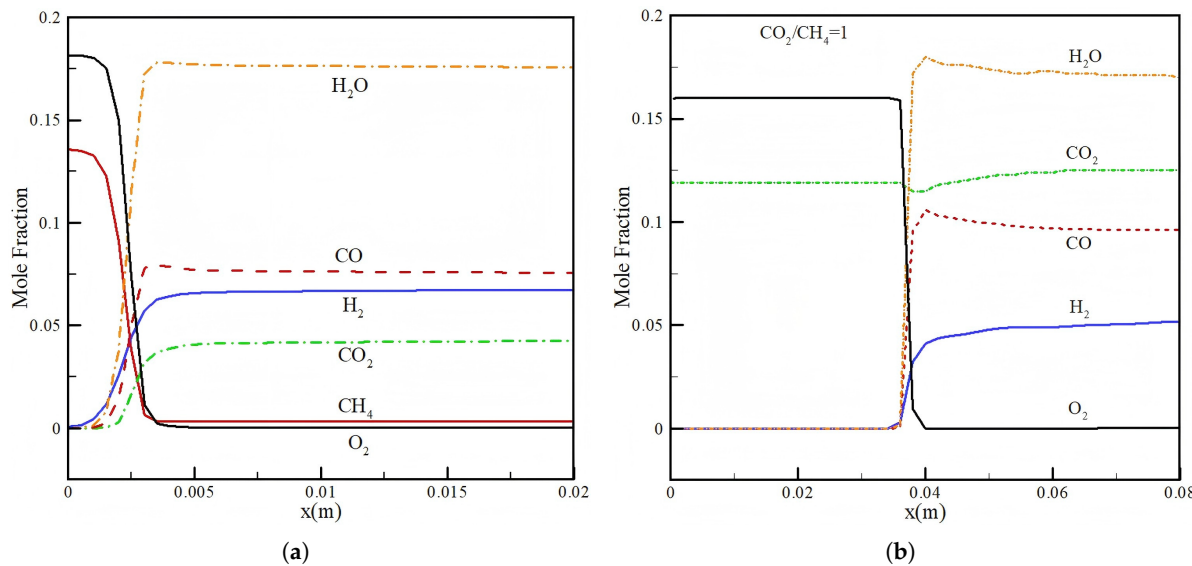


Figure 3. The distribution of major species near the reaction zone. (a) $\text{CO}_2/\text{CH}_4 = 0$. (b) $\text{CO}_2/\text{CH}_4 = 1$.

Figure 4 presents the molar fraction of the main syngas components in the products and the conversion efficiency for different molar ratios of CO_2/CH_4 , with experimental results included for comparison.

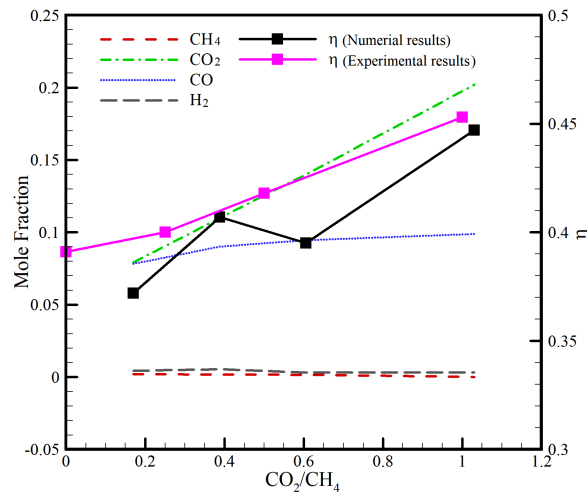


Figure 4. The molar fraction of major species and reforming efficiency for different CO_2 dilution concentrations [14].

It can be observed from the figure that the numerical results in this study show good agreement with the experimental data. The experimental results indicate that conversion efficiency increases with higher molar ratios of CO_2/CH_4 . However, predictions show a significant drop in reforming efficiency at a CO_2/CH_4 ratio of 0.5. This discrepancy may

be attributed to the model used in this study. We employed the volume-averaged method for modeling, which could lead to deviations between the predictions and experimental results. Additionally, the predictions utilize GRI 1.2 rather than the most recent chemical kinetics, which may also contribute to the observed deviations.

As the molar ratio of CO_2/CH_4 increases, the molar fractions of CO_2 and CO rise, while the molar fraction of H_2 slightly decreases. Although the molar fraction of CO_2 at the outlet increases, the net production of CO_2 decreases because CO_2 participates in the reverse reaction of water to gas, namely $\text{CO}_2 + \text{H}_2 \leftrightarrow \text{H}_2\text{O} + \text{CO}$. In this reaction, H_2 also acts as a reactant, leading to the formation of CO and a consequent reduction in H_2 concentration. As the CO_2/CH_4 ratio increases from 0 to 1, the conversion efficiency of methane/air improves from 37.1% to 44.7%.

3.2. Effect of Heat Loss

Figure 5 shows the temperature curves of gas and solid phases under different heat loss coefficients. The heat loss coefficient, denoted as β , was experimentally evaluated to be $330 \text{ W}/(\text{m}^3 \cdot \text{K})$ for a well-insulated porous burner [25]. The experimental values of Zeng et al. [14] are also shown for comparison. For the molar ratio of $\text{CO}_2/\text{CH}_4 = 0$, the numerical results for $\beta = 1000 \text{ W}/(\text{m}^3 \cdot \text{K})$ and $\beta = 2000 \text{ W}/(\text{m}^3 \cdot \text{K})$ are in good agreement with the experimental values. With the increase in β , the heat loss through the wall to the surroundings increases, and the temperatures of gas and solid phases decrease, which are obviously lower than Zeng's experimental values. When the molar ratio of CO_2/CH_4 is 0 and β exceeds $1000 \text{ W}/(\text{m}^3 \cdot \text{K})$, the flame propagates downstream and finally moves out to the reactor outlet. This phenomenon is not shown in Figure 5 for the sake of clarity. This β value is defined as a critical value for stable combustion in the reactor. For the molar ratio of $\text{CO}_2/\text{CH}_4 = 1$, the critical value of β is $2500 \text{ W}/(\text{m}^3 \cdot \text{K})$. This is consistent with the results of Shi et al. [17] that the wall heat loss should not exceed 70% of the total heat of the reactor. The flame propagates downstream by predictions for $\text{CO}_2/\text{CH}_4 = 1$ with different heat loss coefficients compared to the experiments. This discrepancy may stem from the inappropriate heat loss coefficient applied in the computations.

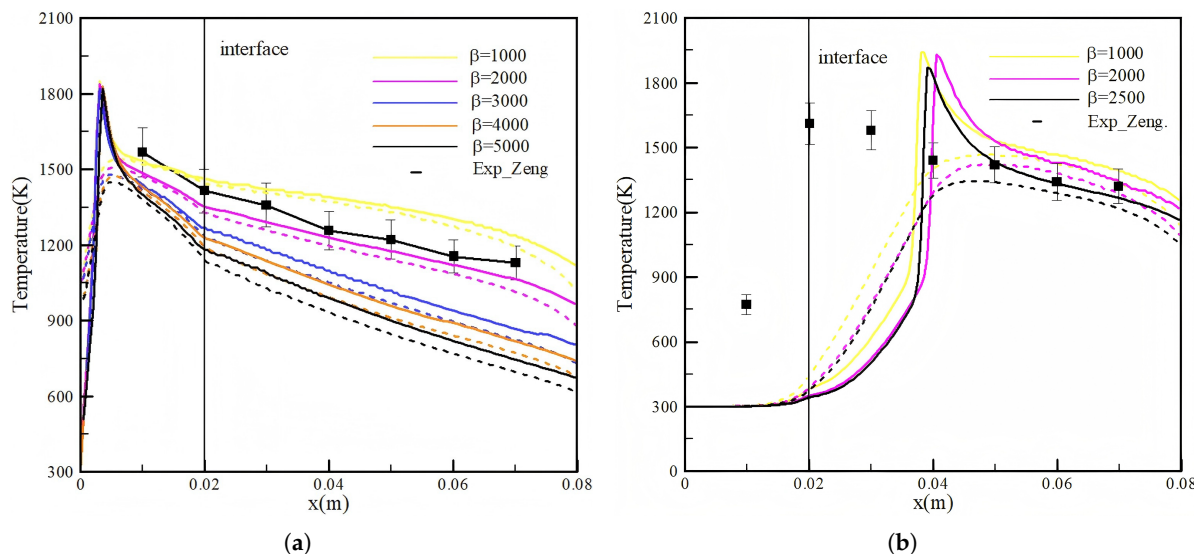


Figure 5. Temperature distributions for different β (solid line is gas temperature T_g ; dashed line is solid temperature T_s). (a) $\text{CO}_2/\text{CH}_4 = 0$. (b) $\text{CO}_2/\text{CH}_4 = 1$.

Figure 6 shows the molar fractions of the main syngas components in the products and conversion efficiency as a function of β for molar ratios of $\text{CO}_2/\text{CH}_4 = 0$ and 1.

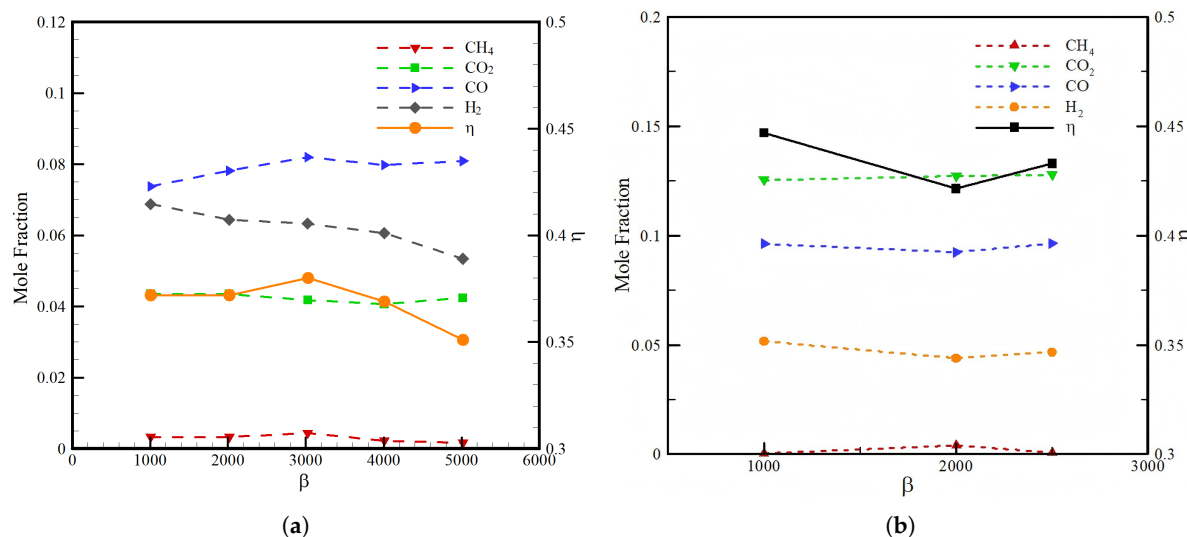


Figure 6. Major syngas and reforming efficiency as a function of β . (a) $\text{CO}_2/\text{CH}_4 = 0$. (b) $\text{CO}_2/\text{CH}_4 = 1$.

It can be observed from the figure that the increase in β leads to a decrease in the temperatures of gas and solid phases. At the same time, a decrease in the molar fraction of H_2 and a slight increase in the molar fraction of CO are observed as β is increased. However, the conversion efficiency decreases with β , which indicates that a greater conversion can be obtained for the lower β .

3.3. Effect of Thermal Conductivity

In the packing bed, the gas–solid convective heat transfer coefficient and thermal conductivity are very important for heat transfer in a porous media reactor. The effects of thermal conductivity on the temperature distribution of gas and solid phases and the conversion efficiency of syngas are discussed. In this study, the heat loss coefficient $\beta = 1000 \text{ W}/(\text{m}^3 \cdot \text{K})$ and the solid surface emissivity $\xi = 0.8$ are kept unchanged, while λ_s is varied.

Figure 7 shows the temperature distributions with $\text{CO}_2/\text{CH}_4 = 0.5$ for different solid thermal conductivities. The thermal conductivity of the benchmark is $0.32 \text{ W}/(\text{m} \cdot \text{K})$. As shown in Figure 7, the thermal conductivity of the solid has little effect on the gas temperature, but it has an obvious effect on the solid's temperature. The effective thermal conductivity of the packing bed consists of two parts, which are the thermal conductivity of solid material λ_s and radiative thermal conductivity λ_{rad} . With the increase in λ_s , the heat conduction in the packing bed is enhanced, the solid temperature gradient becomes smaller, the preheating effect of the fresh mixture in the upstream is reduced, and the flame moves downstream. For $\lambda_s = 0.16 \text{ W}/(\text{m} \cdot \text{K})$, the flame is located at the interface of two porous media.

Table 1 presents the main components of syngas in the products and the conversion efficiency. It can be observed that the lowest molar fractions of H_2 and CO are obtained for the benchmark thermal conductivity value of $0.32 \text{ W}/(\text{m} \cdot \text{K})$. When λ_s is increased from $0.32 \text{ W}/(\text{m} \cdot \text{K})$ to $0.64 \text{ W}/(\text{m} \cdot \text{K})$, the conversion efficiency increases from 39.5% to 42.9%. However, further increase in λ_s from $0.64 \text{ W}/(\text{m} \cdot \text{K})$ to $1.28 \text{ W}/(\text{m} \cdot \text{K})$ leads to a negligible decrease in conversion efficiency. This indicates that increases in λ_s lead to a slight increase in conversion efficiency.

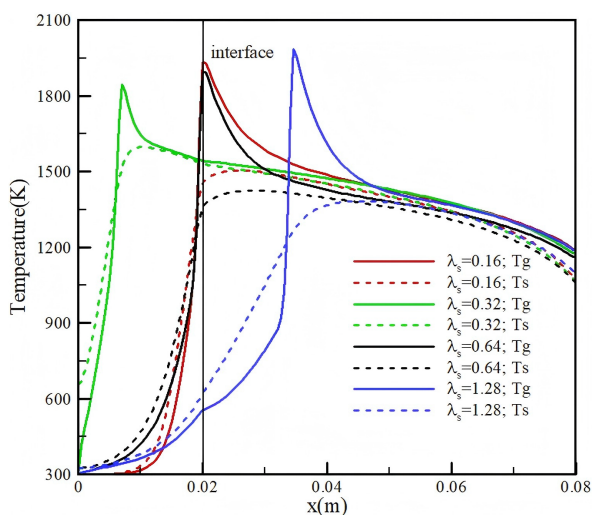


Figure 7. Temperature distributions for different λ_s ($\text{CO}_2/\text{CH}_4 = 0.5$, $\beta = 1000 \text{ W}/(\text{m}^3 \cdot \text{K})$, $\xi = 0.8$).

Table 1. Molar fraction of major species and reforming efficiency for different λ_s ($\text{CO}_2/\text{CH}_4 = 0.5$, $\beta = 1000 \text{ W}/(\text{m}^3 \cdot \text{K})$, $\xi = 0.8$).

$\lambda_s (\text{W/m} \cdot \text{K})$	X_{CO_2}	X_{H_2}	X_{CO}	X_{CH_4}	$\eta (\%)$
0.16	0.0867	0.0584	0.0894	0.0031	41.7
0.32	0.0838	0.0515	0.0885	0.0024	39.5
0.64	0.0894	0.0634	0.0870	0.0019	42.9
1.28	0.0857	0.0612	0.0897	0.0031	42.5

4. Conclusions

The partial oxidation of rich fuels in porous media is a promising technology for supplying the syngas used in solid oxide fuel cells. In this paper, a one-dimensional steady-state model of a two-layer porous media reactor is established and the detailed chemical reaction mechanism of GRI-Mech 1.2 is used to study the partial combustion of methane/air with injection of CO_2 in the mixture. The effects of molar ratio of CO_2/CH_4 , heat loss coefficient and solid thermal conductivity on gas and solid temperature distribution, syngas production, and conversion efficiency are analyzed. The main conclusions are as follows:

1. Injection of CO_2 into methane/air mixture can improve the conversion efficiency. As the CO_2/CH_4 ratio increases from 0 to 1, the conversion efficiency of the methane/air mixture improves from 37.1% to 44.7%;
2. The conversion efficiency decreases from 0.15 to 0.12 when the heat loss coefficient is increased from $1000 \text{ W}/(\text{m}^3 \cdot \text{K})$ to $2000 \text{ W}/(\text{m}^3 \cdot \text{K})$;
3. The thermal conductivity of porous media primarily affects the temperature of the solid and the conversion efficiency. When the thermal conductivity is increased from $0.32 \text{ W}/(\text{m} \cdot \text{K})$ to $0.64 \text{ W}/(\text{m} \cdot \text{K})$ for a molar ratio of $\text{CO}_2/\text{CH}_4 = 0.5$, the conversion efficiency increases from 39.5% to 42.9%.

Author Contributions: Conceptualization: X.W.; methodology: X.W.; formal analysis and investigation: X.W., M.Y., Z.L. and Z.W.; writing—original draft preparation: X.W.; writing—review and editing: X.Z., J.S., X.K. and J.L.; funding acquisition: X.Z. and J.S.; supervision: X.Z. All authors have read and agreed to the published version of the manuscript.

Funding: This research was supported by the National Natural Science Foundation of China (NSFC Grant No. 51876107).

Data Availability Statement: The original contributions presented in this study are included in the article. Further inquiries can be directed to the corresponding author.

Acknowledgments: The authors are grateful to many colleagues with whom they had the privilege to interact and collaborate over the years and whose work is partially referenced in this article.

Conflicts of Interest: The authors declare that the research was conducted in the absence of any commercial or financial relationships that could be construed as potential conflicts of interest.

Nomenclature

Symbol	Definition
c_g	specific heat capacity, $\text{J}\cdot\text{kg}^{-1}\cdot\text{K}^{-1}$
d	the diameter of the ball, mm
h_k	the molar enthalpy of component i , $\text{J}\cdot\text{mol}^{-1}$
h_v	the volume convective heat transfer coefficient
M	mole fraction
Nu	Nusselt number
P	pressure, Pa
Pr	Prandtl number
Re	Reynolds number
T	temperature, K
u	gas velocity, $\text{m}\cdot\text{s}^{-1}$
W_k	molecular weight of the k component
Y_k	mass fraction of component k
$\dot{\omega}_k$	the reaction rate of the k component
β	heat loss coefficient, $\text{W}\cdot\text{m}^{-3}\cdot\text{K}^{-1}$
ε	porosity
η	conversion efficiency
λ_{eff}	effective thermal conductivity, $\text{W}\cdot\text{m}^{-1}\cdot\text{K}^{-1}$
λ_{rad}	radiative thermal conductivity, $\text{W}\cdot\text{m}^{-1}\cdot\text{K}^{-1}$
λ_s	thermal conductivity for solid, $\text{W}\cdot\text{m}^{-1}\cdot\text{K}^{-1}$
ρ	density, $\text{kg}\cdot\text{m}^{-3}$
σ	Stefan–Boltzmann constant, $\text{W}\cdot\text{m}^{-2}\cdot\text{K}^{-4}$
ξ	surface emissivity of porous media

References

- Al-Hamamre, Z.; Al-Zoubi, A. The use of inert porous media based reactors for hydrogen production. *Int. J. Hydrogen Energy* **2010**, *35*, 1971–1986. [[CrossRef](#)]
- Toledo, M.G.; Utria, K.S.; González, F.A.; Zuñiga, J.P.; Saveliev, A.V. Hybrid filtration combustion of natural gas and coal. *Int. J. Hydrogen Energy* **2012**, *37*, 6942–6948. [[CrossRef](#)]
- Dhamrat, R.S.; Ellzey, J.L. Numerical and experimental study of the conversion of methane to hydrogen in a porous media reactor. *Combust. Flame* **2006**, *144*, 698–709. [[CrossRef](#)]
- Wang, Y.; Zeng, H.; Shi, Y.; Cao, T.; Cai, N.; Ye, X.; Wang, S. Power and heat co-generation by micro-tubular flame fuel cell on a porous media burner. *Energy* **2016**, *109*, 117–123. [[CrossRef](#)]
- Smith, C.H.; Leahey, D.M.; Miller, L.E.; Ellzey, J.L. Conversion of wet ethanol to syngas via filtration combustion: An experimental and computational investigation. *Proc. Combust. Inst.* **2011**, *33*, 3317–3324. [[CrossRef](#)]
- Dorofeenko, S.O.; Polianczyk, E.V. Conversion of hydrocarbon gases to synthesis gas in a reversed-flow filtration combustion reactor. *Chem. Eng. J.* **2016**, *292*, 183–189. [[CrossRef](#)]
- Fan, L.; Li, C.; Aravind, P.V.; Cai, W.; Han, M.; Brandon, N. Methane reforming in solid oxide fuel cells: Challenges and strategies. *J. Power Sources* **2022**, *538*, 231573. [[CrossRef](#)]
- Fukuhara, C.; Yamamoto, K.; Makiyama, Y.; Kawasaki, W.; Watanabe, R. A metal-honeycomb-type structured catalyst for steam reforming of methane: Effect of preparation condition change on reforming performance. *Appl. Catal. A* **2015**, *492*, 190–200. [[CrossRef](#)]
- Bingue, J.P.; Saveliev, A.V.; Fridman, A.A.; Kennedy, L.A. Hydrogen production in ultra-rich filtration combustion of methane and hydrogen sulfide. *Int. J. Hydrogen Energy* **2002**, *27*, 643–649. [[CrossRef](#)]
- Toledo, M.; Gracia, F.; Caro, S.; Gómez, J.; Jovicic, V. Hydrocarbons conversion to syngas in inert porous media combustion. *Int. J. Hydrogen Energy* **2016**, *41*, 5857–5864. [[CrossRef](#)]

11. Toledo, M.; Bubnovich, V.; Saveliev, A.; Kennedy, L. Hydrogen production in ultrarich combustion of hydrocarbon fuels in porous media. *Int. J. Hydrogen Energy* **2009**, *34*, 1818–1827. [[CrossRef](#)]
12. Araya, R.; Araus, K.; Utria, K.; Toledo, M. Optimization of hydrogen production by filtration combustion of natural gas by water addition. *Int. J. Hydrogen Energy* **2014**, *39*, 7338–7345. [[CrossRef](#)]
13. Zeng, H.Y.; Wang, Y.Q.; Shi, Y.X.; Cai, N.S. Experimental study for partial oxidation reforming of CH₄/CO₂ with rich combustion in a porous media burner. *J. Eng. Thermophys.* **2017**, *38*, 2269–2275.
14. Zeng, H.; Wang, Y.; Shi, Y.; Ni, M.; Cai, N. Syngas production from CO₂/CH₄ rich combustion in a porous media burner: Experimental characterization and elementary reaction model. *Fuel* **2017**, *199*, 413–419. [[CrossRef](#)]
15. Jiang, L.; Liu, H.; Suo, S.; Xie, M.; Bai, M. Simulation of propane-air premixed combustion process in randomly packed beds. *Appl. Therm. Eng.* **2018**, *141*, 153–163. [[CrossRef](#)]
16. Jiang, L.; Liu, H.; Wu, D.; Wang, J.; Xie, M.Z.; Bai, M. Pore-scale simulation of hydrogen-air premixed combustion process in randomly packed beds. *Energy Fuels* **2017**, *31*, 12791–12803. [[CrossRef](#)]
17. Shi, J.; Mao, M.; Li, H.; Liu, Y.; Deng, Y. Influence of chemical kinetics on predictions of performance of syngas production from fuel-rich combustion of CO₂/CH₄ mixture in a two-layer burner. *Front. Chem.* **2020**, *7*, 902. [[CrossRef](#)]
18. Shi, J.; Mao, M.; Li, H.; Liu, Y.; Sun, Y. Pore-level study of syngas production from fuel-rich partial oxidation in a simplified two-layer burner. *Front. Chem.* **2019**, *7*, 793. [[CrossRef](#)]
19. Shi, J.; Mao, M.; Li, H.; Liu, Y.; Lv, J. A pore level study of syngas production in two-layer burner formed by staggered arrangement of particles. *Int. J. Hydrogen Energy* **2020**, *45*, 2331–2340. [[CrossRef](#)]
20. Zheng, C.; Cheng, L.; Cen, K.; Bingue, J.P.; Saveliev, A. Partial oxidation of methane in a reciprocal flow porous burner with an external heat source. *Int. J. Hydrogen Energy* **2012**, *37*, 4119–4126. [[CrossRef](#)]
21. Alenazey, F.; Alyousef, Y.; AlOtaibi, B.; Almutairi, G.; Minakshi, M.; Cheng, C.K.; Vo, D.-V.N. Degradation behaviors of solid oxide fuel cell stacks in steady-state and cycling conditions. *Energy Fuels* **2020**, *34*, 14864–14873. [[CrossRef](#)]
22. Bowman, C.T.; Hanson, R.K.; Davidson, D.F.; Gardiner, W.C.; Lissianski, J.V.; Smith, G.P.; Golden, D.M.; Frenklach, M.; Goldenberg, M. GRI-Mech 3.0 Chemical Kinetic Mechanism. Combustion Research Group at Berkeley. 2009. Available online: <http://combustion.berkeley.edu/gri-mech/new21/version12/text12.html> (accessed on 6 September 2023).
23. Kee, R.J.; Dixon, G.L.; Warnatz, J.; Coltrin, M.E.; Miller, J.A. *A Fortran Computer Code Package for the Evaluation of Gas-Phase Multicomponent Transport Properties; Report SAND86-8246*; Sandia National Laboratories: Albuquerque, NM, USA, 1986.
24. Barra, A.J.; Diepvens, G.; Ellzey, J.L.; Henneke, M.R. Numerical study of the effects of material properties on flame stabilization in a porous burner. *Combust. Flame* **2003**, *134*, 369–379. [[CrossRef](#)]
25. Contarin, F.; Saveliev, A.; Fridman, A.; Kennedy, L.A. Reciprocal flow filtration combustor with embedded heat exchangers: Numerical study. *Int. J. Heat Mass Transf.* **2003**, *46*, 949–961. [[CrossRef](#)]

Disclaimer/Publisher’s Note: The statements, opinions and data contained in all publications are solely those of the individual author(s) and contributor(s) and not of MDPI and/or the editor(s). MDPI and/or the editor(s) disclaim responsibility for any injury to people or property resulting from any ideas, methods, instructions or products referred to in the content.